

# Novel Modulation Schemes for Conventional and Sparse Matrix Converters Facilitating Reactive Power Transfer Independent of Active Power Flow

Frank Schafmeister and Johann W. Kolar

ETH Zurich, Power Electronic Systems Laboratory  
 ETH Zentrum / ETL H17, Physikstr. 3, CH-8092 Zurich / SWITZERLAND  
 Tel.: +41-1-632 6493 Fax.: +41-1-632 1212  
 email: schafmeister@lem.ee.ethz.ch

**Abstract.** Two novel modulation schemes are proposed which facilitate the transfer of reactive power from the load side to the mains side of a three-phase AC-AC Sparse Matrix Converter (SMC) or a Conventional Matrix Converter. The derivation of the modulation schemes which rely on a decoupling of the output voltage and the input current formation is described in detail. Furthermore, the operating limits concerning modulation index and reactive current magnitude are determined. Finally, all theoretical considerations are verified by digital simulations and measurements on a 7.5kW prototype of a Very Sparse Matrix Converter.

## 1 Introduction

Sparse Matrix Converter (SMC, cf. Fig.1) systems [1] are functionally equivalent to Conventional Matrix Converters (CMC) but are characterized by a lower realization effort and a lower control complexity and are therefore especially interesting for an industrial application.

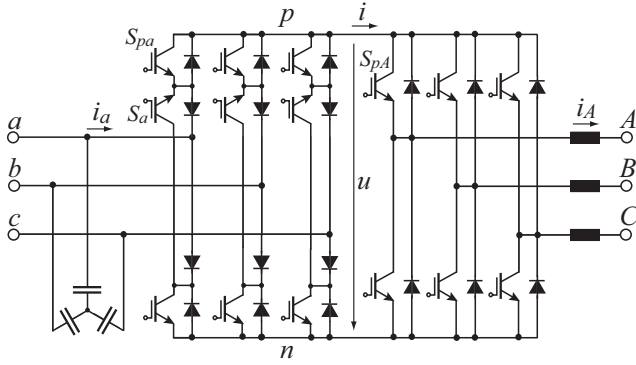


Fig.1: Topology of the Sparse Matrix Converter (SMC) according to [1].

Within each pulse half period two line-to-line voltages are switched into the DC link of the SMC by proper control of the input stage (cf. Fig.2). There, the input stage commutation is at zero current (cf.  $i$  in Fig.2, or Fig.6 in [1], [2]) what allows to avoid a multi-step commutation which has to be performed in dependency on the sign of the commutating voltage or commutating current for the CMC and/or results in low switching losses and high converter reliability.

Modulation schemes facilitating the transfer of a reactive current  $i_2 = j \cdot i_{2q}$ , from the load side to the converter input are not known from literature so far. Therefore, e.g. the reactive current of an asynchronous machine operating at no load cannot not be used for compensating the capacitive reactive current drawn by the input filter capacitors.

In this paper, two novel modulation schemes are proposed which are facilitating the transfer of reactive power from the load side to the mains side of the converter what facilitates a significant extension of the application area of SMC and/or CMC systems.

For achieving a reactive power transfer, the switching cycle of conventional SMC modulation scheme (cf. Fig.2) resulting in the well-known voltage and current time behavior (cf. Fig.3),

has to be extended by additional intervals for reactive current formation. In a second step, both partial intervals can be merged into a combined modulation scheme, which can be implemented in a corresponding algorithm. It is important to note that this extension of conventional modulation is not limited to the SMC, but can also be transferred to the CMC.

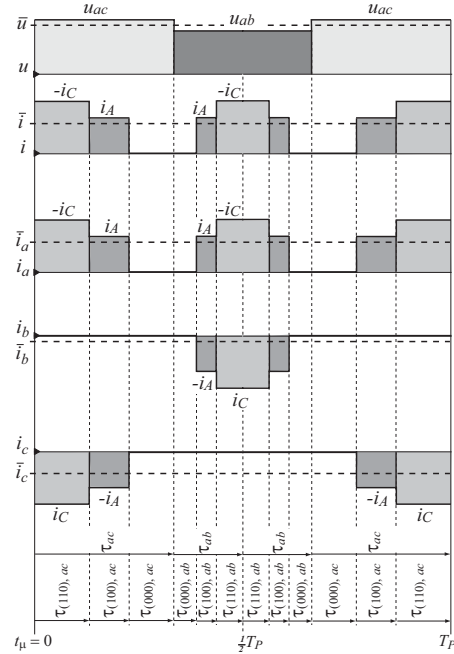


Fig.2: Conventional SMC Modulation Scheme (cf. Fig.9 in [1]); time behavior of  $u$ ,  $i$ , and the mains phase currents  $i_a, i_b, i_c$ , within a pulse period  $t_p=0 \dots T_p$  for  $\varphi_1$  in  $0 \dots +\pi/6$  and  $\varphi_2$  in  $+\pi/6 \dots +\pi/3$ . This corresponds to the current space vector diagram shown in Fig.5 for input, i.e.  $\underline{i}_1$  (local average value), and output, i.e.  $\underline{i}_2$ , being in phase with the respective voltages  $\underline{u}_1$  and  $\underline{u}_2$  (local average value), i.e.  $\Phi_1 = \Phi_2 = 0$ .  $\varphi_2$  denotes the phase of the reference value of the output voltage space vector. For the sake of clarity a low pulse frequency is assumed and the ripple components of  $u$  and  $i$  are neglected.

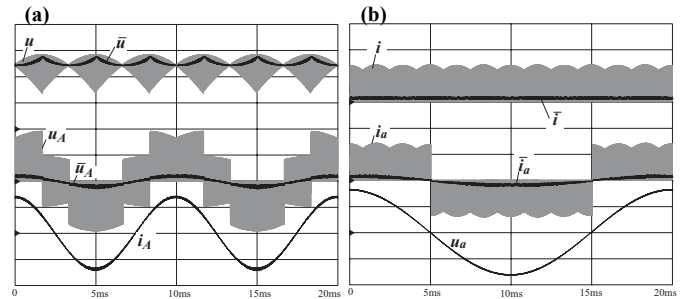


Fig.3: Simulation of the SMC operating behavior for conventional modulation and  $\Phi_1 = \Phi_2 = 0$  (cf. Fig.2). (a) voltage formation, DC-link voltage and voltage of output terminal A; (b) current formation, DC-link current and input current  $i_a$ . Scales: 200V/div, 15A/div; modulation index  $M_{12}=0.1$ ,  $f_1=50\text{Hz}$ ,  $f_2=100\text{Hz}$ .

As shown in **Section 2**, with conventional modulation no input current fundamental can be formed for purely reactive load ( $\Phi_2=\pi/2$ ). In **Section 3** the novel modulation schemes facilitating a reactive power transfer from the load to the input/mains and/or the formation of a desired reactive input current ( $\Phi_1=\pm\pi/2$ ) in case of  $\Phi_2=\pi/2$  are described. **Section 4** compares the operating limits of the proposed modulation schemes. Furthermore, an exact analytical description of the limits in dependency on the system operating parameters is provided. Simulation results as well as measurements gained from a VSMC prototype and validating the proposed modulation schemes are given in **Section 5**. Finally, possible applications of the novel modulation schemes are discussed in **Section 6**.

## 2 Effects of Conventional Modulation Schemes on Converter Operation with Reactive Load

According to [1], [2], [3] we have for the relative turn-on times of the single switching states of the SMC (and/or CMC) for  $\phi_1$  in  $-\pi/6 \dots +\pi/6$  and  $\phi_2$  in  $0 \dots +\pi/3$  with  $M_{12}:=2/\sqrt{3} \hat{U}_2/\hat{U}_1$

$$\begin{aligned} d_{ab} &= \cos(\phi_1 + \pi/3) \\ d_{ac} &= \cos(\phi_1 - \pi/3) \\ \delta_{(100)} &= M_{12} \cdot \cos(\phi_2 + \pi/6) \\ \delta_{(110)} &= M_{12} \cdot \sin(\phi_2) \end{aligned} \quad (1)$$

$$\begin{aligned} \delta_{(100),ac} &= d_{ac} \cdot \delta_{(100)} \\ \delta_{(110),ac} &= d_{ac} \cdot \delta_{(110)} \\ \delta_{(110),ab} &= d_{ab} \cdot \delta_{(110)} \\ \delta_{(100),ab} &= d_{ab} \cdot \delta_{(100)} \end{aligned} \quad (2)$$

The above given relationships finally result in pulse patterns<sup>1</sup> like shown for  $\Phi_1=\Phi_2=0$  in Fig.2 and for  $\Phi_2=\pi/2$  in **Fig.4**. The time behavior of the DC-link current  $i$  and of the input phase currents differs considerably for both cases. This is caused by the different phase displacement  $\Phi_2$  of the output voltage and current fundamentals. As shown in detail in [1] and [5], current segments  $-i_C$  with negative sign are occurring in  $i$  for  $\Phi_2 > \pi/6$  as the projection of the vector  $\underline{i}_2$  onto the (110)-axis then shows negative values for certain angles  $\phi_2$  within the load voltage period (cf. Fig.5a).

Two special cases are occurring for the conventional pulse pattern if (A) either the load is purely reactive, i.e.  $\underline{i}_2 = j \cdot i_{2q}$  ( $\Phi_2 = \pm\pi/2$ ) or (B) a purely reactive behavior of the input current fundamental  $\hat{i}_1^* = j \cdot i_{1q}$  ( $\Phi_1^* = \pm\pi/2$ ) should be achieved.

### A. Purely Reactive Load, $\Phi_2 = \pi/2$

The time behavior of characteristic voltages and currents for purely reactive load is shown in Fig. 4. The corresponding space vector diagram is depicted in **Fig. 5b**.

Subsequently always two current segments showing equal ampere seconds but inverse signs are switched into the DC-link. This results in a zero local average value of the DC link current and of the input phase currents. Accordingly, for  $\Phi_2 = \pi/2$  no fundamental of the input current can be formed. This can be verified geometrically also from Fig.5b, as, e.g. for  $\phi_2=\pi/3$  exclusively  $-i_C$  is switched into the DC link where  $i_{C,\phi_2=\pi/3}=0$  is valid. Furthermore, one could refer to [1], [4] where the amplitude of the input current fundamental has been calculated as

$$\hat{I}_1 = \frac{\sqrt{3}}{2} M_{12} \hat{I}_2 \cdot \cos(\phi_2) \quad (3)$$

<sup>1</sup> In all figures absolute turn-on times  $\tau$  are shown, which are related to the duty cycle  $\delta$  via  $\tau = \delta \cdot \frac{1}{2} T_P$ .

which results in  $\hat{I}_1=0$  for  $\cos\phi_2=0$ .

### B. Purely Reactive Power at Converter Input, $\Phi_1^* = -\pi/2$

Another special operating condition is given for  $\Phi_1^* = -\pi/2$  (and/or  $\Phi_1^* = +\pi/2$ ). In this case<sup>2</sup> – in analogy to the operation with a purely reactive power demand of the load, as described above, volt-seconds of same magnitude but inverse sign do occur at the output terminals, i.e.: for  $\Phi_1^* = -\pi/2$  no local average value and/or fundamental of the output voltage can be formed.

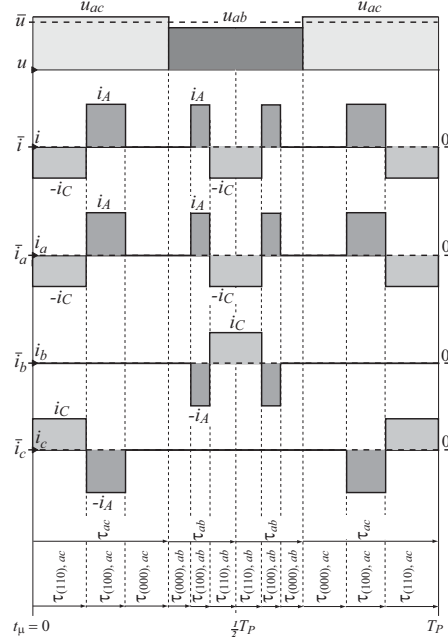


**Fig.4:** Conventional modulation scheme; time behavior of  $u$ ,  $i$ , and of the mains phase currents  $i_a, i_b, i_c$ , within a pulse period  $t_\mu=0 \dots T_P$ . Assumed system operating conditions equal as for Fig.2 but  $\Phi_2=\pi/2$  (cf. Fig. 5b,  $\Phi_1=0$ ). The positive and negative current-time-areas switched subsequently into the DC link are exactly compensating each other, accordingly no zero local average value of the input phase currents results.

This can be verified geometrically in Fig.5a or with reference to [1] using

$$\hat{U}_2 = \frac{\sqrt{3}}{2} M_{12} \hat{U}_1 \cdot \cos(\phi_1^*) \quad (4)$$

As there is no fundamental of the load voltage, no load current fundamental will be present and/or the input current will show zero fundamental amplitude.

### C. Combining Cases A and B

By directly combining the two above described special operating conditions, i.e. purely reactive power at the output and at the input of the converter leads to the well-known dilemma: For  $\Phi_2 = +\pi/2$  and  $\Phi_1^* = -\pi/2$  (cf. Figs.5a and b) neither an output voltage nor an input current formation is possible. Therefore, in summary, no reactive power can be transferred from the converter output to the input in case conventional modulation is employed.

Nevertheless, this combination of special cases can be used to solve the problem of reactive power transfer. The proposed basic approach utilizes the fact, that on one hand in case (A) the input current formation is not affected by the output voltage formation and on the other hand in case (B) the output voltage formation is not

<sup>2</sup> To facilitate this type of operation, quasi-negative DC-link voltages have to be applied by inverting the switching state of the inverter stage; cf. Section 3.B and Section V.A.1 in [1].

affected by the (reactive) input current formation. This means, input current and output voltage can be formed independently from each other in two subsequent steps. There, the only modification to be considered is the need of a DC link current showing an average value unequal to zero for the duration while both (reactive) input current forming vectors  $((ba), (ac))$  in Fig.5a and/or  $((ba), (bc))$  in Fig. 8a) are applied. This requirement can be met by temporarily switching the largest output phase current into the DC link.

### 3 Novel Modulation Schemes for Transferring Reactive Power from the Output to the Input

#### A. Basic Principle Based on Separation of Output Voltage and Input Current Formation

For the following considerations the load is assumed to draw a purely inductive current,  $\Phi_2 = +\pi/2$ . Accordingly, considering a power balance we have for the input current  $\Phi_1 = -\pi/2$ . Referring to Section 2.A, in this case the input current formation is not affected by the conventional modulation, i.e. the input current local average value is equal to zero.

Now, the basic idea of the proposed modified modulation schemes [6] is to utilize each second pulse half period for the formation of reactive current at the input side what – according to the above given considerations – will not affect the output voltage. This is equivalent to a decoupling of the output voltage formation and input current formation, which allows to separately adjust both quantities according to different set points. It will be shown in the following that this principle is feasible even though certain limits are given.

#### B. Transferring Reactive Power using Two Input Current Vectors

Figure 5a visualizes the construction of the DC-link voltage for conventional modulation which is used for each first half of a pulse period and utilizes always the two highest positive line-to-line input voltages  $u_{ac}$  and  $u_{ab}$ . Furthermore, it illustrates the separate formation of the reactive current vector  $\hat{I}_{1q}^*$  from the two corresponding discrete input current vectors  $(ab)$  and  $(ac)$  within the second half of each switching cycle. Thereby, both discrete current vectors are formed by the phase current of the output stage, showing the maximum instantaneous value (here:  $-i_B$ ). It should be mentioned that the effectively required negative input current vector  $(ba)$  is realized by impressing the maximum negative output phase current (here:  $i_B$ ) which is obtained by inverting the switching state of the output stage (to  $(010)$ ) (cf. Section V.A.1 in [1]).

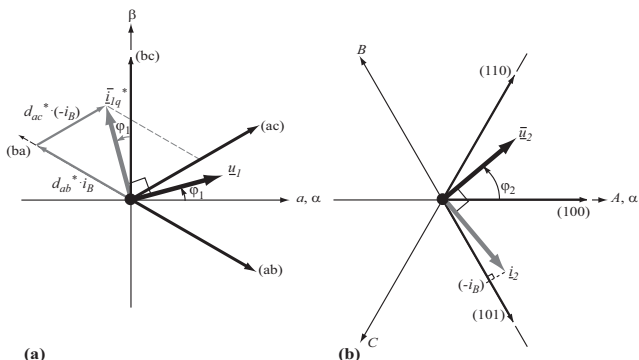


**Fig.5:** Space vector diagrams of (a) input stage and (b) output stage valid for purely reactive power transfer between input and output. The formation of the local average value  $\hat{I}_{1q}^*$  of the reactive input current from discrete vectors  $(ba)$  and  $(ac)$  as shown in (a) characterizes the „Two-Vector-Scheme“.

The pulse pattern corresponding to the space vector diagram shown in Fig.5 is depicted in Fig.6. The voltage and current formation performed in the first and second half of the pulse period can be

clearly recognized. Since the modulation employs only two discrete input current vectors (and/or DC-link voltage levels) it is denoted as „Two-Vector-Scheme“.

In the following the derivation of analytical expressions for the relative turn-on times  $d_{ab}^*$  and  $d_{ac}^*$  of the second, reactive current forming pulse half period is described briefly. Formulating the geometrical relations of Fig.5a yields

$$\frac{\sin(\pi/3 - \varphi_1)}{d_{ac}^* \cdot i_{2,max}} = \frac{\cos(\varphi_1 + \pi/6)}{d_{ac}^* \cdot (-i_B)} = \frac{\sin(\pi/3)}{\hat{I}_{1q}^*}$$

$$\frac{\sin(\pi/3 + \varphi_1)}{d_{ba}^* \cdot i_{2,max}} = \frac{\cos(\varphi_1 - \pi/6)}{d_{ba}^* \cdot i_B} = \frac{\sin(\pi/3)}{\hat{I}_{1q}^*}$$

with

$$i_B = \hat{I}_2 \cdot \cos(\varphi_2 - 2\pi/3 - \pi/2) = -\hat{I}_2 \cdot \cos(\varphi_2 - \pi/6). \quad (6)$$

Accordingly, we then have for the relative turn-on times

$$d_{ab}^* = \frac{2}{\sqrt{3}} \frac{\hat{I}_{1q}^*}{\hat{I}_2} \cdot \frac{\cos(\varphi_1 - \pi/6)}{\cos(\varphi_2 - \pi/6)}$$

$$d_{ac}^* = \frac{2}{\sqrt{3}} \frac{\hat{I}_{1q}^*}{\hat{I}_2} \cdot \frac{\cos(\varphi_1 + \pi/6)}{\cos(\varphi_2 - \pi/6)}$$

In order not to take influence on the formation of the output voltage by inserting additional current pulses

$$d_{ac}^* \cdot u_{ac} - d_{ab}^* \cdot u_{ab} = 0. \quad (8)$$

has to be fulfilled (cf. Fig.6). With

$$u_{ac} = \sqrt{3} \cdot \hat{U}_1 \cdot \cos(\varphi_1 - \pi/6) \quad (9)$$

$$u_{ab} = \sqrt{3} \cdot \hat{U}_1 \cdot \cos(\varphi_1 + \pi/6)$$

the validity of (8) is given inherently. Hence, the output voltage and input current formation are decoupled what verifies the basic principle of the modulation method.

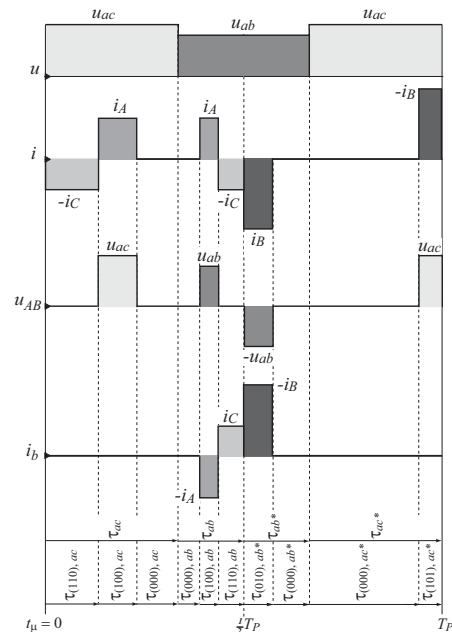


**Fig.6:** Modulation scheme comprising an output voltage and a reactive input current forming pulse half period. In both intervals only two different input current vectors  $((ac)$  and  $(ab))$  and/or line-to-line input voltages (DC-link voltages  $u_{ac}$  and  $u_{ab}$ ) are applied; accordingly the modulation method is denoted as „Two-Vector-Scheme“. Obviously, the volt seconds added to the output voltage (e.g.:  $u_{AB}$ ) during the second half of the pulse period are equal to zero, while during the first half of the pulse period no local current average value is generated in any of the input phases (e.g.:  $i_b$ ).

Furthermore, it should be pointed out that (8) is equivalent to zero average DC link power transfer within the second pulse half period. Since only reactive power has to be transferred via the DC link the

local average value  $p$  of the active power has to equal zero. E.g., we have for the second half of the pulse period  $p = u_{ac} d_{ac}^* (-i_B) + u_{ab} d_{ab}^* i_B$ ; considering (8) this directly results in  $p = 0$ .

The voltage and current pulses resulting from the separate voltage and current formation (cf. Fig.6) can be combined into a single pulse pattern of lower duration and/or an increased output voltage modulation range as described briefly in [3]. In case only a low reactive current has to be transferred, the full converter modulation range is available.

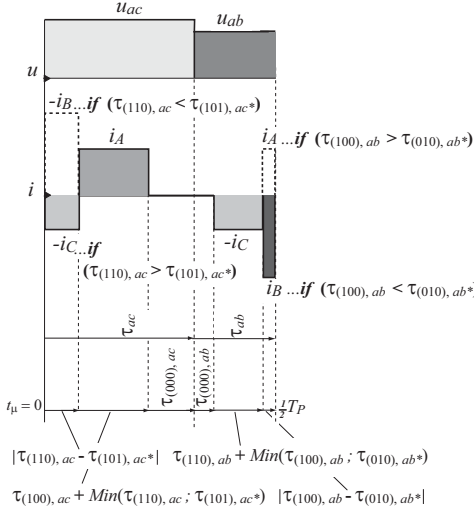


**Fig.7:** Final pulse pattern resulting for the „Two-Vector-Scheme“ after merging both halves of the pulse period depicted in Fig. 6.

Incorporating two additional pulses with widths  $d_{ab}^*$  and  $d_{ac}^*$ , the application of the modulation scheme shown in Fig.6 will result in a significant reduction of the output voltage modulation range, since the effective duration of the voltage formation interval is reduced by the sum of  $d_{ab}^* + d_{ac}^*$ .

The voltage modulation range can be regained within certain limits (cf. Section 4), if the voltage and current pulses resulting from the separate voltage and current formation pulse half intervals (cf. Fig.6) are combined into a single pulse pattern of lower duration which is depicted in Fig.7. The interval merging is based on the consideration two current pulses of inverse polarity appearing for the same DC-link voltage level can be added (e.g.,  $(-i_B) + (-i_C)$ ). This results in a pulse of larger widths of the third output phase current (e.g.,  $i_A$ ). Thus the duration of one of the two original current pulses of the voltage formation interval is reduced while the duration of the second current pulse is extended. So, in case only a small reactive current has to be transferred, the full converter modulation range is available.

### C. Transferring Reactive Power using Three Input Current Vectors

The formation of a reactive current at the converter input side can also be performed utilizing the discrete current vectors which are close to the sector of the desired average current vector. This is illustrated in Fig. 8a for the example already discussed in Fig.5; in the case at hand the vectors  $(ba)$  and  $(bc)$  are used for forming the reactive input current  $\hat{I}_{lq}^*$ .

Fig. 9 depicts the corresponding pulse pattern again consisting of voltage- and current-forming pulse half periods. Now, in total three different input current vectors or DC-link voltage levels are applied: the output voltage formation is realized by  $(ac)$  and  $(ab)$  in the first half of a pulse period, subsequently  $(ab)$  and  $(bc)$  are applied for reactive input current formation in the second half of the pulse period. Accordingly, the modulation method is denoted as „Three-Vector-Scheme“ in the following.

The switching state turn-on times  $d_{ab}^*$  and  $d_{bc}^*$  of the

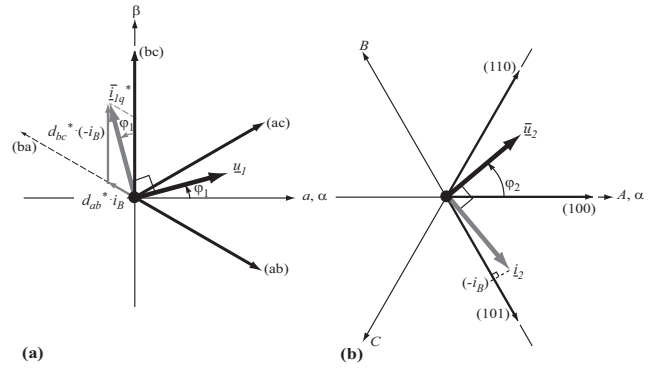


**Fig.8:** Space vector diagrams of (a) input stage and (b) output stage valid for purely reactive power transfer between converter input and output. The formation of the reactive input current vector  $\hat{I}_{lq}^*$  (local average value) using vectors  $(ba)$  and  $(bc)$  as shown in (a) characterizes the „Three-Vector-Scheme“ (for output voltage formation  $(ac)$  and  $(ab)$  are utilized, so in total 3 different vectors are employed within each pulse period).

input current formation interval can be derived in analogy to the „Two-Vector-Scheme“ as

$$\frac{\sin(\varphi_1)}{d_{ba}^* \cdot i_{2,max}} = \frac{\sin(\varphi_1)}{d_{ab}^* \cdot i_B} = \frac{\sin(2\pi/3)}{\hat{I}_{lq}^*} \quad (10)$$

$$\frac{\sin(\pi/3 - \varphi_1)}{d_{bc}^* \cdot i_{2,max}} = \frac{\cos(\varphi_1 + \pi/6)}{d_{bc}^* \cdot (-i_B)} = \frac{\sin(2\pi/3)}{\hat{I}_{lq}^*}$$

what leads for  $\varphi_1 > 0$  with (6) to

$$d_{ab}^* = \frac{2}{\sqrt{3}} \frac{\hat{I}_{lq}^*}{\hat{I}_2} \cdot \frac{\sin(\varphi_1)}{\cos(\varphi_2 - \pi/6)} \quad (11)$$

$$d_{bc}^* = \frac{2}{\sqrt{3}} \frac{\hat{I}_{lq}^*}{\hat{I}_2} \cdot \frac{\cos(\varphi_1 + \pi/6)}{\cos(\varphi_2 - \pi/6)}$$

Analogously,  $\varphi_1 < 0$  yields

$$d_{ac}^* = \frac{2}{\sqrt{3}} \frac{\hat{I}_{lq}^*}{\hat{I}_2} \cdot \frac{\sin(|\varphi_1|)}{\cos(\varphi_2 - \pi/6)} \quad (12)$$

$$d_{cb}^* = \frac{2}{\sqrt{3}} \frac{\hat{I}_{lq}^*}{\hat{I}_2} \cdot \frac{\cos(|\varphi_1| + \pi/6)}{\cos(\varphi_2 - \pi/6)}$$

Due to the changed sign for  $\varphi_1$  the negative current pulse  $i_B$  now has to be assigned to  $d_{cb}^*$  and not to  $d_{ab}^*$  (as for  $\varphi_1 > 0$ ). With

$$u_{bc} = \sqrt{3} \cdot \hat{U}_1 \cdot \sin(\varphi_1) \quad (13)$$

the decoupling condition

$$d_{bc}^* \cdot u_{bc} - d_{ac}^* \cdot u_{ac} = 0 \quad (14)$$

(for  $\varphi_1 > 0$ ) is fulfilled what verifies the basic function of the „Three-Vector-Scheme“.

As illustrated in Fig.10 for the „Three-Vector-Scheme“ a merging of current and voltage pulses is possible only for the input stage switching state appearing in both pulse half intervals (in the case at hand  $(ab)$ ). This results on one hand in a reduction of the output voltage modulation range, but on the other hand, only a comparably low turn-on time of the current vectors is required for forming a desired average input current (cf. Fig.6 and Fig.9):

$$d_{ab,2V}^* = d_{ab,3V}^* + d_{bc,3V}^* \quad (15)$$

$$d_{ac,2V}^* = d_{bc,3V}^*$$

Accordingly, the reactive current transfer ratio ( $\hat{I}_{lq}^* / \hat{I}_2$ ) could be increased by a factor of up to  $\sqrt{3}$  as compared to the „Two-Vector-Scheme“ for low output voltage.

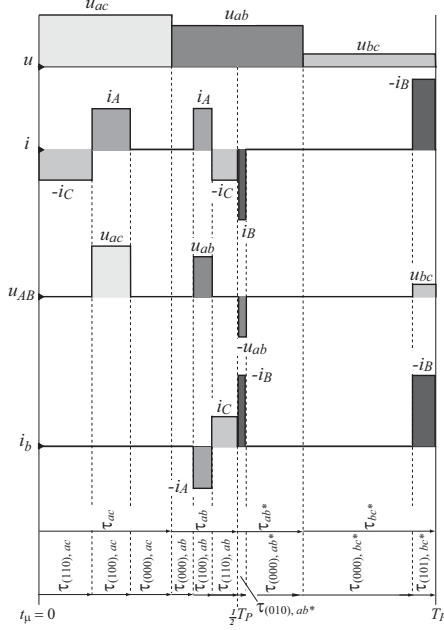


**Fig.9:** Modulation based on the „*Three-Vector-Scheme*“. In total three different input current vectors and/or DC-link voltage levels (*ac*), (*ab*), (*bc*) are employed within each pulse period.

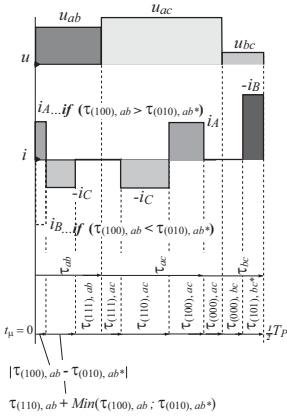


**Fig.10:** Modulation scheme resulting for the „*Three-Vector-Scheme*“ after merging input current pulses and/or output voltage pulses occurring for  $u=u_{ab}$  being present in both halves of the pulse period depicted in Fig.9. *Remark:* Changing the sequence of the voltage pulses forming  $u$  as compared to Fig.9 allows reaching a subsequent level of  $u$  by changing only the switching state of either the upper or the lower half of the converter input stage and therefore does minimize the control complexity.

#### 4 Transfer Limits of the Proposed Modulation Schemes

For a practical application the operating limits of the proposed modulation schemes are of special interest. E.g. for the „*Three-Vector-Scheme*“ the sum of all relative turn-on times of a pulse half period is

$$d_{tot,3V} = \delta_{(110),ac} + \delta_{(100),ac} + \left| \delta_{(100),ab} - d_{ab}^* \right| + \delta_{(110),ab} + \text{Min}(\delta_{(100),ab}, d_{ab}^*) + d_{bc}^* \quad (16)$$

where the reactive current transfer limit  $MI_{max}$  is reached for  $d_{tot,3V}=1$ .

In this section the limits of the operating range of the proposed modulation schemes as determined numerically using a search algorithm are discussed. Furthermore, the analytical calculation of the operating limits will be shown for the „*Three-Vector-Scheme*“.

##### A. Basic Method for Determining the Operating Limits

According to (16)  $d_{tot,3V}$  depends on four variables, i.e.  $M_{12}$ ,  $MI$ ,  $\varphi_1$ , and  $\varphi_2$  where

$$MI := \frac{\hat{I}_{1q}^*}{\hat{I}_2} \quad (17)$$

denotes the reactive current transfer ratio. For determining the relevant  $MI_{max}$  corresponding to  $d_{tot}=1$  the maximum of  $d_{tot}$  (cf. (16)) in  $\varphi_1$  and  $\varphi_2$  has to be found in order to ensure  $d_{tot} \leq 1$  within the whole mains or load period. There, one has to notice that the locations of the maxima of  $d_{tot}$  change with varying  $M_{12}$  and  $MI$ . Therefore, a numerical algorithm was employed for determining the maximum reactive current transfer ratio  $MI_{max}$  over the full range of  $M_{12}$ . The resulting dependency of  $MI_{max}$  on  $M_{12}$  is shown for both modulation schemes in Fig.11.

##### B. Comparison of the Modulation Schemes

As already mentioned in Section 3.C, the *Three-Vector-Scheme* is clearly superior for small output voltages and/or low modulation indices  $M_{12}$ . For  $M_{12}=0$  the ratio  $\hat{I}_{1q,max}/\hat{I}_2$  is  $3/4$ , compared to  $\sqrt{3}/4$  for the *Two-Vector-Scheme*.

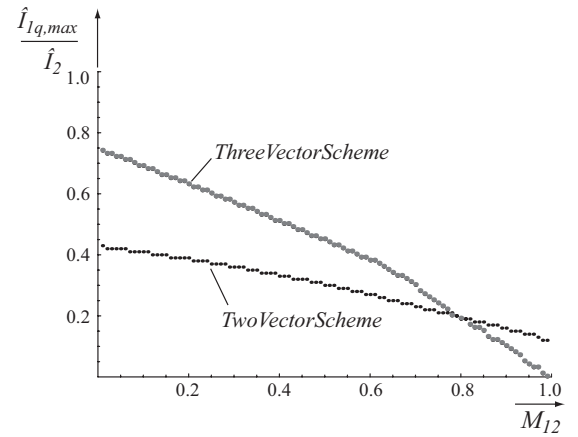


**Fig.11:** Operating limits concerning the formation of the output voltage and the reactive input current for the proposed modulation schemes.

For high  $M_{12}$  the application of the *Two-Vector-Scheme* is advantageous, since it allows  $\hat{I}_{1q,max}/\hat{I}_2 = 1/8$  even at maximum output voltage ( $M_{12}=1$ ), while the *Three-Vector-Scheme* due to the on-time of the additionally inserted third input current vector is unable to transfer reactive current at  $M_{12}=1$ . The intersection of both limits is at  $M_{12}=4/5=0.8$  (and  $MI=1/5$ ), thus in order to achieve an optimal reactive current transfer the modulation has to be switched from *Three-* to *Two-Vector-Scheme* for  $M_{12}>0.8$ .

##### C. Analytical Determination of the Limits

The numerically calculated transfer limits can be verified by analytical considerations based on plausible limiting conditions as shown in the following.

###### C.1 Three-Vector-Scheme

The limitation of the modulation range can be found analytically considering two plausible limiting conditions. The first condition is relevant for small  $M_{12}$  and therefore determined by the current limit. Analogously, the second limit is significant for large  $M_{12}$ , i.e. it is determined by the voltage limit.

###### I. Vicinity of Current Limit

For an output phase displacement of  $\varphi_2 = \pi/2$  the output phase current which can be switched into the DC link and/or is available for forming a reactive input current is minimum for an output voltage angle of e.g.  $\varphi_2=\pi/3$ . So this output angle determines the current limit for any  $M_{12}$ , while the critical input voltage angle  $\varphi_1$  varies with  $M_{12}$ :

$$\begin{aligned}\varphi_{1,crit} &= \varphi_{1,crit}(M_{12}, MI) \\ \varphi_{2,crit} &= \pi/3 \Rightarrow \delta_{(100)} = 0\end{aligned}\quad (18)$$

Hence, (16) yields

$$d_{tot,3V,I} = \delta_{(110),ac} + \delta_{(110),ab} + d_{ab}^* + d_{bc}^* \quad (19)$$

and finally

$$d_{tot,3V,I} = \frac{\sqrt{3}}{2} M_{12} \cdot \cos(\varphi_1) + \frac{4}{3} MI \cdot \cos(\varphi_1 - \pi/6). \quad (20)$$

The maximum of  $d_{tot,3V,I}$  in  $\varphi_1$  now could be determined using

$$\frac{\partial d_{tot,I}}{\partial \varphi_1} := 0 \quad (21)$$

resulting in

$$\varphi_{1,crit}(M_{12}, MI) = \arccos\left(\frac{\sqrt{3}(3M_{12} + 4MI)}{\sqrt{27M_{12}^2 + 72M_{12}MI + 64MI^2}}\right) \quad (22)$$

which represents the point of time within a mains period where overmodulation occurs first. Insertion of (22) in (20) and setting

$$d_{tot,3V,I} \Big|_{\varphi_{1,crit}} \equiv 1 \quad (23)$$

(where no freewheeling interval is remaining) finally yields the desired interrelation between modulation index and maximum reactive transfer ratio for small  $M_{12}$

$$MI_{max,3V,I} = \frac{3}{16} (\sqrt{16 - 3M_{12}^2} - 3M_{12}). \quad (24)$$

## II. Vicinity of Voltage Limit

The maximal achievable output voltage transfer ratio is determined by the input voltage angle  $\varphi_1=0$  and the output voltage angle  $\varphi_2=\pi/6$  (in this case no free wheeling intervals are remaining at the modulation limit). So, neither the critical input- nor the critical output voltage angle varies with  $M_{12}$

$$\varphi_{1,crit} = 0 \quad (25)$$

$$\varphi_{2,crit} = \pi/6$$

Considering (25), (16) yields

$$d_{tot,3V,II} = \delta_{(110),ac} + \delta_{(100),ac} + \delta_{(100),ab} + \delta_{(110),ab} + d_{bc}^* \quad (26)$$

and finally

$$d_{tot,3V,II} = M_{12} + MI. \quad (27)$$

The modulation limit for large  $M_{12}$  is again determined by

$$d_{tot,3V,II} \equiv 1$$

and results to

$$MI_{max,3V,II} = 1 - M_{12}. \quad (28)$$

Equating (24) and (28) leads to the modulation index limit

$$M_{12,Lim} = \frac{2}{19} (14 - 3\sqrt{7}) \approx 0.638 \quad (29)$$

defining the sharp bend in Fig.11 and characterizing the transition from (24) to (28) (cf. Fig.12).

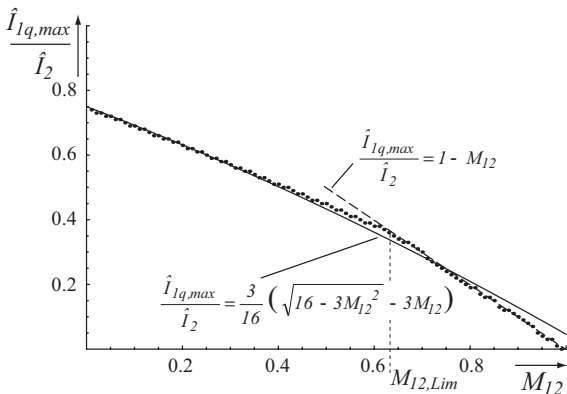


**Fig.12:** Analytically calculated and numerically gained transfer limit of the Three Vector Modulation Scheme show an excellent consistency.

All equations given above are verified by the numerical results from section 4.B and show an excellent consistency (cf. Fig.12).

## C.2 Two-Vector-Scheme

### I. Vicinity of Current Limit

For the *Two-Vector-Scheme*

$$MI_{max,2V,I} = \frac{1}{16} (\sqrt{48 - 27M_{12}^2} - 3M_{12}) \quad (30)$$

can be derived for small  $M_{12}$  in analogy to (24).

### II. Vicinity of Voltage Limit

Analogously to (28)

$$MI_{max,2V,II} = \frac{1}{2} \left[ 1 - \frac{3}{4} M_{12} \right] \quad (31)$$

can be found for large  $M_{12}$ . Accordingly,

$$M_{12,Lim} = \frac{2}{3} \quad (32)$$

characterizes the transition from (30) to (31). Also in this case the analytical results are in excellent consistency with the numerically gained transfer limit.

## 5 Digital Simulation and Experimental Results

The proposed modulation schemes and the operating limits are verified by digital simulation using *SIMPLORER* (cf. Fig.13).

For, e.g.  $M=0.2$  and  $MI=0.38$  ( $\hat{I}_1 = MI \cdot \hat{I}_2$ , cf. (17)) the amplitude of the input phase current  $\hat{I}_a$  shows the expected value. It should be pointed out that the DC link current  $i$  resulting for the formation of reactive input current does show a local average value  $\bar{i}$ , in contrary to conventional modulation. This, however, is not connected to an average active power flow  $\bar{p}$  as has been shown in Section 3.B ( $\bar{p}=0$  is valid within each pulse period).

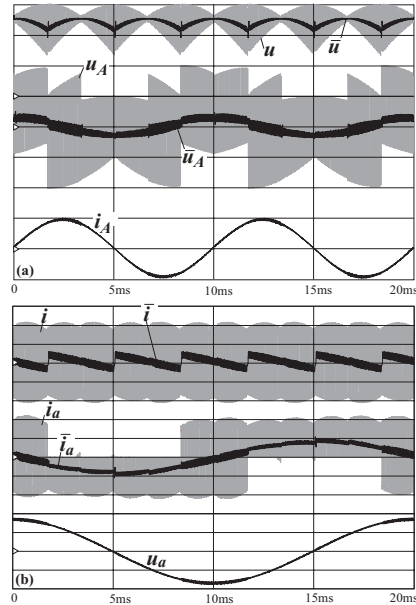


**Fig.13:** Digital simulation of the operating behavior of the SMC with purely reactive current transfer from the output to the input stage for  $\Phi_1 = -\pi/2$  and  $\Phi_2 = +\pi/2$ ; modulation as shown in Fig.7. Parameters:  $U_f = 170V$ ,  $f_1 = 50Hz$ ,  $f_2 = 100Hz$ ,  $f_r = 15kHz$ ,  $L_{Load} = 25mH$ ,  $M = 0.2$ ,  $MI = 0.38$ . Scales: (a): 100V/Div, 2A/Div; (b): 100V/Div, 1A/Div.

Experimental results also clearly verify the proposed modulation schemes. Fig.14 shows the characteristic quantities measured on a SMC prototype operated with the *Two-Vector-Scheme* and for the same operating parameters as defined for the system simulation in Fig.14. One has to notice, that the measured amplitude  $\hat{I}_1$  of the fundamental of the reactive input current exceeds the theoretical (and simulated) value by  $\Delta \hat{I}_1 \approx 300mA$ . This difference is due to the reactive current drawn by the input filter capacitors which is present also in case of conventional modulation. This influence of the input filter was excluded from the simulation model in order to clearly show the transfer of reactive current from the output to the input.

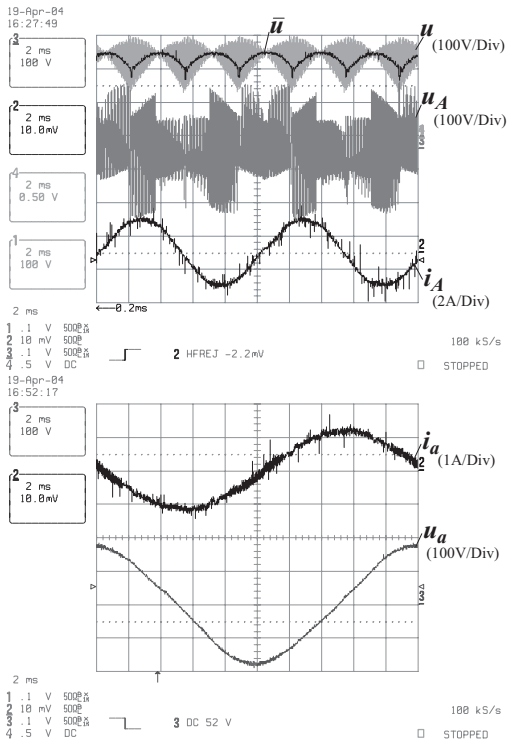


**Fig.14:** Experimental results gained from a SMC prototype operated with the *Two-Vector-Scheme*. (a): Representation as for Fig.13a; (b): input phase voltage  $u_a$  and low-pass filtered input phase current  $i_a$  showing a phase displacement of  $\Phi_j = -\pi/2$ . System parameters and scales as for Fig.13.

## 6 Conclusions

The transfer of reactive power via the DC-link of a CMC and a SMC is advantageous for several applications. E.g. it facilitates the sinusoidal guidance of the output voltage of a SMC in boost-mode (as recently proposed in [3], cf. **Fig.15**) independent of the load condition. When operating the SMC in buck-mode it allows compensating the reactive power of the input filter also for purely reactive load like given, e.g. in case feeding an asynchronous machine operating in no-load condition.

In this paper two novel modulation schemes, i.e. the *Two-Vector-* and *Three-Vector-Scheme* are proposed for transferring reactive current from the SMC/CMC output to the input. There, the basic idea is a decoupling of the output voltage and reactive input current formation. The schemes are identical to conventional modulation within each first half of a pulse period, the second half of a pulse period is used for the formation of a desired reactive input current. The individual pulses of a pulse period are finally merged into a single pulse pattern what results in an increased modulation range. As compared to the *Two-Vector-Scheme* the *Three-Vector-Scheme* facilitates a higher reactive current transfer ratio  $\hat{I}_{1q,max}/\hat{I}_2$  for low output voltages and/or in the lower modulation range up to  $M_{12} = 0.8$ . For  $M_{12} > 0.8$  the *Two-Vector-Scheme* is advantageous since it allows  $\hat{I}_{1q,max}/\hat{I}_2 = 1/8$  even for maximum output voltage, i.e.  $M_{12} = 1.0$ .

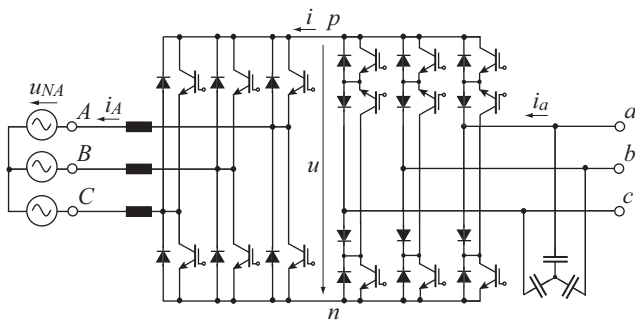


**Fig.15:** Operation of a SMC in boost mode. The definition of the positive voltage and current directions is assumed equal as for conventional (buck-mode) operation in Fig.1.

## References

- [1] Kolar, J.W., Baumann, M., Schafmeister, F., and Ertl, H.: *Novel Three-Phase AC-DC-AC Sparse Matrix Converter, Part I and II*. Proceedings of the 17th Annual IEEE Applied Power Electronics Conference, Dallas (Texas), USA, March 10 - 14, Vol. 2, pp. 777 - 791 (2002).
- [2] Wei, L., and Lipo, T.A.: *A Novel Matrix Converter Topology with Simple Commutation*. Record of the IEEE Industry Applications Society Annual Meeting, Chicago, Sept. 30 - Oct. 4, Vol. 3, pp. 1749-1754 (2001).
- [3] Kolar, J.W., Schafmeister, F.: *Novel Modulation Schemes Minimizing the Switching Losses of Sparse Matrix Converters*. Proceedings of the 29th Annual Conference of the IEEE Industry Electronics Society, Roanoke (VA), USA, Nov. 2 - 6, pp. 2085 - 2090 (2003).
- [4] Huber, L., and Borojevic, D.: *Space Vector Modulation with Unity Input Power Factor for Forced Commutated Cycloconverters*. Record of the 26th IEEE Industry Applications Society Annual Meeting, Dearborn, USA, Sept. 28 - Oct. 4, Vol. I, pp. 1032-1041 (1991).
- [5] Schafmeister, F., Baumann, M., and Kolar, J.W.: *Analytically Closed Calculation of the Conduction and Switching Losses of Three-Phase AC-AC Sparse Matrix Converters*. Proceedings of the 10<sup>th</sup> International Power Electronics and Motion Control Conference, Sept. 9-11, Cavtat & Dubrovnik, Croatia (2002).
- [6] Schafmeister, F., and Kolar, J.W.: *Verfahren zur Kopplung der ein- und ausgangsseitigen Blindleistungsflüsse dreiphasiger Matrixkonverter*. Swiss Patent Application, April 2004.